Chiral Generation of Hot Carriers for Polarization-Sensitive Plasmonic Photocatalysis

Yoel Negrín-Montecelo, Artur Movsesyan, Jie Gao, Sven Burger, Zhiming M Wang, Sylvain Nlate, Emilie Pouget, Reiko Oda, Miguel Comesaña-Hermo, Alexander O Govorov, et al.

Chiral Generation of Hot Carriers for Polarization-Sensitive Plasmonic Photocatalysis

Yoel Negrín-Montecelo,[1,2] Artur Movsesyan,[3,4] Jie Gao,[5] Sven Burger,[6,7] Zhiming M. Wang,[4] Sylvain Nlate,[5] Emilie Pouget,[5] Reiko Oda,[5] Miguel Comesaña-Hermo,[8,*] Alexander O. Govorov,[3,*] and Miguel A. Correa-Duarte[1,2,*]

[1]CINBIO, Universidade de Vigo, Department of Physical Chemistry, 36310 Vigo, España

[2]Instituto de Investigación Sanitaria Galicia Sur (IIS Galicia Sur), CIBERSAM. SERGAS-UVIGO

[3]Department of Physics and Astronomy, Nanoscale and Quantum Phenomena Institute, Ohio University, Athens, Ohio 45701, United States

[4]Institute of Fundamental and Frontier Sciences, University of Electronic Science and Technology of China, Chengdu, 610054, China

[5]Chimie et Biologie des Membranes et des Nanoobjets (CBMN), CNRS, Université de Bordeaux, Bordeaux INP, UMR 5248, 33607, Pessac, France

[6]Zuse Institute Berlin, 14195 Berlin, Germany

[7]JCMwave GmbH, 14050 Berlin, Germany

[8]Université de Paris, CNRS, ITODYS, F-75013 Paris, France

Corresponding authors: miguel.comesana-hermo@u-paris.fr, govorov@ohio.edu, macorrea@uvigo.es

Abstract: Mastering the manipulation of chirality at the nanoscale has long been a priority for chemists, physicists and materials scientists, given its importance in the biochemical processes of the natural world and in the development of novel technologies. In this vein, the formation of novel metamaterials and sensing platforms resulting from the synergic combination of chirality and plasmonics has opened new avenues in nano-optics. Recently, the implementation of chiral plasmonic nanostructures in photocatalysis has been proposed theoretically as a means to drive polarization-dependent photochemistry. In the present work, we demonstrate that the use of inorganic nanometric chiral templates for the controlled assembly of Au and TiO_2 nanoparticles leads to the formation of plasmon-based photocatalysts with polarization-dependent reactivity. The formation of plasmonic assemblies with chiroptical activities induces the asymmetric formation of hot electrons and holes generated via electromagnetic excitation, opening the door to novel photocatalytic and optoelectronic features. More precisely, we demonstrate that the reaction yield can be improved when the helicity of the circularly polarized light used to activate the plasmonic component matches the handedness of the chiral substrate. Our approach may enable new applications in the fields of chirality and photocatalysis, particularly toward plasmon-induced chiral photochemistry.

Introduction: Plasmonic photocatalysis and plasmonic photosensitization of large-bandgap semiconductors involve mechanisms that rely on the formation of highly energetic carriers (i.e., hot electrons and hot holes) upon electromagnetic excitation of plasmonic metal nanoparticles (NPs); such mechanisms are currently under investigation as a means to improve the selectivity and efficiency of many chemical transformations.[1–3] Their implementation in processes with an important societal impact, such as the photoreduction of CO_2 or the production of H_2 through water photolysis, is causing them to gain traction as renewable and affordable energy sources.[4,5] Previous results have demonstrated that harvesting visible and NIR photons through the localized surface plasmon resonance (LSPR) effect can activate large-bandgap semiconductors such as TiO_2 to access a broader range of the electromagnetic spectrum.[6–8] In these examples, the formation of a physical interface (Schottky barrier) is needed in order to ensure an efficient hot electron injection into the conduction band of the semiconductor upon plasmonic excitation. Hot electron transfer is accompanied by the concomitant formation of a hot hole at the Fermi level of the metal that can be used to catalyze photo-oxidation reactions.[9] Moreover, assemblies with strong interparticle plasmonic coupling can produce an increase in the local electromagnetic field enhancement that leads to an improved separation of charges at the interface, thus producing an enhanced photoactivation of the semiconductor.[10] Meanwhile, recent developments in colloidal chemistry have been used to create chiral plasmonic NPs, either as isolated objects or as assemblies, with chiroptical activities.[11–14] It has been predicted and observed that the hot carriers produced in these geometries can be sensitive to the polarization of circularly polarized light (CPL).[15–18] This feature can have important repercussions in photocatalysis, where the design of polarization-dependent processes can pave the way towards a new landscape of chemical reactivity. Accordingly, new chiral photochemical applications, such as detection of chirality at the nanoscale, chiral molecular sensing, chiral growth of nanocrystals or asymmetric photo-transformations of plasmonic assemblies, can be envisaged.

A chiral plasmonic entity responds asymmetrically to left- and right-handed CPL (LCP and RCP, respectively).[19] Such plasmonic materials have very high chiroptical activities, with g-factors (differential absorbance of circularly polarized light divided by the absorbance at the same wavelength) almost reaching 0.3, thus several orders of magnitude higher than those of molecular species.[12] This effect is the result of the unique optoelectronic properties of noble metal NPs, such as their ability to concentrate extremely intense electromagnetic fields on their surfaces. Two general colloidal strategies have been used to design plasmonic

systems with strong chiroptical activity.[20] In the first strategy, the individual plasmonic objects are rendered chiral through the surface functionalization of achiral NPs with chiral molecules.[21] Similarly, chiral ligands (such as peptides or amino acids) or micelles formed in the presence of dissymmetric co-surfactants can also be used in a seeded-growth process, leading to the formation of crystals with morphological chirality.[11,12,19] In the second strategy, achiral resonators are assembled onto a chiral substrate, allowing strong interparticle interactions and the formation of an ensemble with chiroptical activity.[13,14,22–25] Unfortunately, the development of experimental systems in which the activation of hot carriers could be implemented in polarization-dependent photocatalysis remains very limited, being restricted to a few examples in which the correlation between the photocatalytic activity and the hot carriers has not been proven explicitly. Among the few reports found in the literature, Hao and coworkers describe the efficiency of a photoreaction induced by chiral plasmonic resonators: Au-gap-Ag nanostructures possessing chiroptical activity from L- or D-cysteine introduced in their gaps exhibit an photocatalytic response that depends on the polarization of the incident light.[21] With a different approach, Saito and Tatsuma reported the formation of chiral plasmonic structures through the selective photodeposition of PbO_2 onto Au nanocuboids.[26] Based on electron microscopy measurements and electromagnetic simulations, the authors attribute the chiroptical behavior to the anisotropic electric field distributions on the achiral metallic objects under CPL and the subsequent site-selective deposition of the dielectric material, which leads to the bottom-up formation of chiral nanostructures. As discussed before, these works are not supported by a theoretical model that unambiguously correlates the photocatalytic activity of the objects with the formation of hot carriers. Such a strategy would allow an easier engineering of chiroptical plasmonic systems and the implementation of the asymmetric response of their hot carriers for the photochemical applications mentioned above.

In the present study, we assembled Au and TiO_2 NPs onto chiral colloidal inorganic substrates, leading to the formation of materials with chiroptical activity (Scheme 1a). To synthesize these substrates, we build on previous studies on the formation of nanometric helical silica structures[27,28] and their functionalization with spherical Au NPs, leading to the formation of a hybrid material in which the grafted plasmonic objects follow the chiral surface of the substrate.[13] Herein, the electrostatic adsorption of TiO_2 NPs will allow the formation of a metal-semiconductor photocatalyst with chiral features, in which the hot electron injection across the Schottky barrier will be sensitive to the polarization of the incident light due to the chiroptical character of the

plasmon signal of the ensemble (Scheme 1b). The phototransformation of rhodamine B (RhB) has been chosen as model photocatalytic reaction in order to demonstrate the asymmetric response of the hot carriers with respect to the helicity of CPL. In this manner, simple spectroscopic techniques will allow us to correlate the photodegradation of the organic dye with the efficiency of the hot electron injection mechanism at the metal-semiconductor interface. Moreover, the experimental data are complemented by numerical simulations and a theoretical formalism that support the characterization of the broadband generation of hot carriers with strong chiroptical activity.

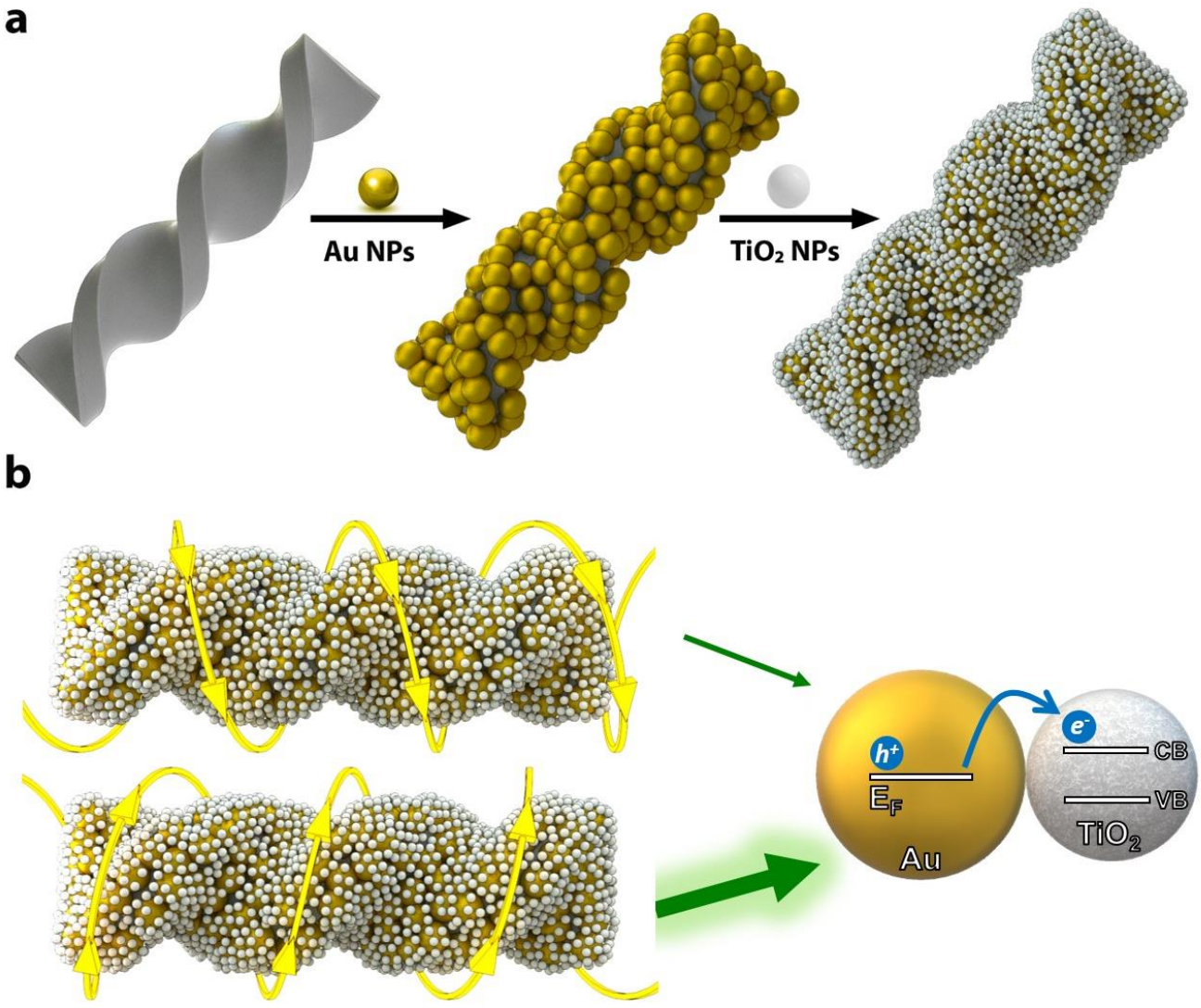

Scheme 1. Chiral colloidal assembly of photocatalytic nanoribbons. Schematics of (a) the adsorption of Au and TiO_2 NPs onto chiral SiO_2 nanoribbons and (b) the asymmetric interaction between a L-handed hybrid and LCP/RCP light. When the helicity of the NP assembly matches that of the CPL, the hot electron transfer between the Fermi level of the metal and the conduction band of the semiconductor is maximized.

Results and discussion: To fabricate experimentally the proposed photocatalytic nanoribbons, we first synthesize twisted SiO_2 nanoribbons with controlled handedness (right (R)- or left (L)-handed) by polycondensation of silanes onto self-assembled organic structures of gemini surfactants with L- or R-tartrate counterions, respectively (Figure 1a, f). These twisted nanoribbons have a width of 21 nm (Figure S2) and a fragmentation step induced by sonication allows the formation of individualized objects in suspension (for experimental details, please refer to the Supporting Information (SI)). Importantly, solid SiO_2 substrates show improved mechanical properties and can even be dispersed in polar organic solvents without loss of structural integrity, in opposition to biomolecular assemblies such as peptides or DNA origami.[29,30] The SiO_2 nanoribbons are subsequently functionalized with amine groups, then pre-synthesized 11 nm spherical Au NPs are covalently grafted on their surfaces, leading to the formation of a hybrid in which the grafted plasmonic objects follow the chiral surface of the twisted nanoribbons (Figure 1b, g, S3a). Along these lines, we have chosen to work with 11 nm Au NPs given their high interparticle coupling efficiencies when adsorbed onto the chiral substrates with respect to smaller objects.[13] Consistent with previous reports, these materials, denoted SiO_2@Au, present a LSPR centered at ~540 nm that corresponds to the absorption dipole of spherical objects (dashed lines in Figure 1d). The R- and L-handed SiO_2@Au hybrids show strong Cotton coupling circular dichroism (CD) signals with opposite signs. L-SiO_2@Au presents a positive maximum at 526 nm and a negative maximum at 585 nm (red dashed lines in Figure 1e), whereas R-SiO_2@Au presents a negative maximum at 525 nm and a positive maximum at 580 nm (blue dashed lines in Figure 1e). For both samples, sign reversal is observed at ~546 nm. Accordingly, the interparticle optical coupling originated from the assembly of the plasmonic resonators onto the chiral inorganic substrate leads to strong chiroptical activities in the visible range of the electromagnetic spectrum.

In the second step of the experimental fabrication, the electrostatic assembly of 5 nm TiO_2 NPs (anatase phase) onto SiO_2@Au leads to the deposition of a superficial layer of semiconductor NPs (SiO_2@Au@TiO_2) that is accompanied by the formation of a Schottky barrier with the metallic component (Figure 1c, h, S3b and S4). This last characteristic ensures an efficient hot electron injection between the Fermi level of Au and the conduction band of TiO_2. For such objects, the slight redshift in the extinction signature (maximum centered at ~550 nm) is accompanied by a small damping in the intensity (full lines in Figure 1d), which is ascribed to the modifications of the dielectric environment surrounding the plasmonic component.[31] The CD response

also shows a redshift in the maxima: the signals are centered at 533 and 594 nm for the L-SiO_2@Au@TiO_2 hybrids and at 531 and 588 nm for R-SiO_2@Au@TiO_2 (full lines in Figure 1e). Here, the sign reversal is also shifted to ~555 nm for both samples. The g-factors for these peaks and their graphical representation (g-factor vs $\lambda_{exc.}$) are presented in Figure S5. Given the chiroptical activities attained and the physical interface created between the metallic and semiconductor components, these hybrids are ideal candidates for polarization-sensitive photocatalytic reactions.

We have created a theoretical model based on a higher-order finite-element method in which spherical Au NPs are organized around a twisted ribbon-like structure (SI). We first computed the extinction and CD spectra of these Au NP arrangements (with and without TiO_2) with recently developed electromagnetic JCMsuite software,[32] by using a computational formalism for the optical response that solves the time-harmonic Maxwell's equations. To simplify our computations, we assumed that the chiral Au NP assembly is embedded in an effective homogeneous dielectric medium (n=1.33 for the SiO_2@Au system and n=1.45 for the SiO_2@Au@TiO_2 nanostructure). Both the theoretical extinction spectra and the CD spectra show good overall qualitative agreement with the experimental data (Figure 1). The extinction maxima are centered at 540 nm for the simulated SiO_2@Au system, which shifts to 565 nm when the dielectric constant of TiO_2 is taken into consideration (Figure 1i). The asymmetric shape of the theoretical spectra may be a consequence of the uneven sizes of the gaps created between the NPs to reproduce the experimental morphology. For the CD data, small divergences appear at lower wavelengths; i.e., the high-energy bands of the theoretical CD signals are redshifted with respect to the experimental data for both SiO_2@Au and SiO_2@Au@TiO_2 (Figure 1j). When the simulated model system with Au NPs forming a crystalline order and the real systems are compared, the disordered disposition of the objects, the variation in their density, their polydispersity, the polydispersity of the silica nanoribbons, and the presence of a silica/water interface may have important effects on the absolute values of the g-factors.[13] Both experiments and theory have proven that the SiO_2@Au@TiO_2 hybrids present chiroptical features that will be implemented towards polarization-dependent photocatalysis.

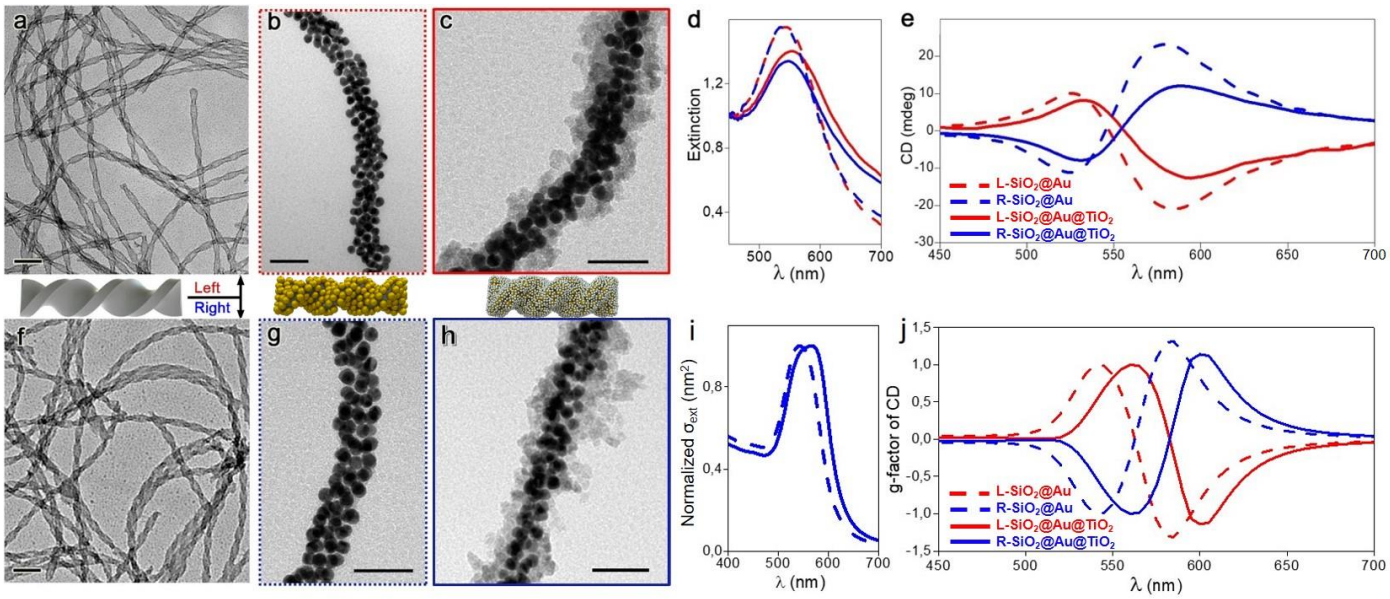

Figure 1. Morphological and optical characterization (both experimental and theoretical data) of the inorganic materials under study. TEM characterization of the L- (a) and R- (f) SiO_2 nanoribbons, L- (b) and R- (g) SiO_2@Au nanoribbons and L- (c) and R- (h) SiO_2@Au@TiO_2 nanoribbons. Experimental (d) and theoretical (i) extinction spectra of the SiO_2@Au and SiO_2@Au@TiO_2 nanoribbons. Experimental (e) and theoretical (j) CD spectra of the SiO_2@Au and SiO_2@Au@TiO_2 nanoribbons. The red and blue colors correspond to the L- and R-enantiomers, respectively. Dashed and full lines correspond to SiO_2@Au and SiO_2@Au@TiO_2 hybrids, respectively. Scale bars correspond to 50 nm. In the calculations, the effective homogeneous dielectric medium is n=1.33 for SiO_2@Au and n=1.45 for SiO_2@Au@TiO_2.

As demonstrated in a previous work,[33] Au-TiO_2 hybrids can act as efficient catalysts of the phototransformation of polycyclic aromatic molecules in aqueous solutions. This reaction proceeds through the formation of reactive oxygen species (ROS), transient molecules generated upon interaction between the hot carriers and water/oxygen molecules. Photocatalytic transformation of such organic substrates under simulated solar radiation can result in complete mineralization or their transformation into fluorescent intermediates. In this work, we take advantage of the same type of model reaction as a simple means to study the polarization-dependent activity of our SiO_2@Au@TiO_2 hybrids. To perform such experiments, either left- or right-handed circular polarizers were inserted into the path of a light source to produce continuous wave excitation in the 400-800 nm region corresponding to the plasmonic range of the hybrids while blocking light below 400 nm (Figure S6). We then evaluated the phototransformation of RhB in the presence of either one of the two SiO_2@Au@TiO_2 enantiomers as a function of irradiation time by using the modified lamp described

above as the CPL source. Herein, the photodegradation rate of the organic dye is directly proportional to the population of hot carriers produced at the metal-semiconductor interface upon plasmonic excitation. The average reaction rates for the phototransformation of RhB were evaluated following $Rate_{experimental}$ = ΔAbsorbance/Δt, where $\Delta t = 8$ hours. When the photocatalytic reaction is performed using L-SiO_2@Au@TiO_2 as the photocatalyst under LCP excitation, we observe an activity value that is 2.93-fold larger with respect to the activity value for the irradiation source with the opposite polarization (Figure 2a, b). Similarly, when RCP light is used to activate R-SiO_2@Au@TiO_2, we observe an activity value that is 2.88-fold larger with respect to the activity value corresponding to LCP under the same conditions (Figure 2c, d). The large enhancement of the polarization-dependent rates is surprising given the relatively small g-factors observed experimentally (see the SI for the related qualitative data). Such result can be considered as a nonlinear photochemical-kinetics effect that leads to an important divergence of the photochemical responses.[34,35] We should emphasize that the optical g-factors (as a linear property) and the photochemical features describe very different properties and are, in general, very different. The chemical kinetics, which lead to the photochemical responses, are intrinsically nonlinear and complex. As previously postulated, photogenerated ROS are responsible for the phototransformation of RhB.[33] Accordingly, the polarization-dependent generation of hot carriers under continuous wave irradiation creates a steady-state population of ROS, whose concentration depends on the coupling between CPL and the handedness of the chiral substrate. Under such premise, even relatively low optical g-factors can produce important differences in the number of ROS molecules photogenerated over time, hence explaining the large variations in photodegradation kinetics between the two light polarizations. In our experiments, we also observed that by switching the polarizer between the two opposite helicities every 8 hours and using L-SiO_2@Au@TiO_2 as the photocatalyst, a drastic decrease in the slope of the reaction profile was observed between LCP and RCP (-1.97 and -0.69, respectively) (Figure 2e). This result demonstrates that the hot electron injection process can be activated or deactivated on demand by inverting the polarization of the incoming light. We evaluated the stability of the materials throughout the photocatalytic tests. For that, we have measured the chiroptical response of R-SiO_2@Au@TiO_2 before and after irradiation as a representative example for both enantiomers. The hybrid nanoribbons remained stable throughout the photocatalytic experiments, and no modification of their CD signals was observed (Figure S7).

The combination of Au and TiO_2 with the formation of a physical interface between them is a necessary component of the experimental design since each material cannot generate the desired polarization-dependent activity when used individually. Several control experiments were performed to corroborate the asymmetric response of the hot carriers. First, the photocatalytic degradation of RhB was performed under the same conditions used in the previous step but manipulating both active components independently (silica nanoribbons decorated either with Au or TiO_2 NPs). We subsequently observed the absence of any noticeable photocatalytic activity in both cases (Figure S8a). This lack of photocatalytic activity confirms that the combination of Au and TiO_2 NPs induces favorable photocatalytic effects that cannot be similarly induced by each material alone. Moreover, the use of L-SiO_2@TiO_2 in the presence of a suspension of 11 nm Au NPs without the formation of a Schottky barrier between the two components, resulted in the same residual photocatalytic activity (Figure S8a). Such results, together with the fact that the photocatalytic experiments were performed at a controlled temperature of 20 °C, exclude any possible interference of thermal contributions in our results.[36] The residual photodegradation of RhB observed in these control experiments is the result of the photobleaching of the organic dye under prolonged photoexcitation (Figure S8b). The same behavior is observed for the L- and R-SiO_2@Au@TiO_2 samples when the handedness of the substrate does not match the helicity of the excitation source (Figure 2). This finding highlights the polarization-dependent character of the hot carriers generated by our photocatalysts when exposed to CPL. In a different set of experiments designed to confirm the role played by the chiral silica support, we studied the photocatalytic performance of achiral hybrids formed by the adsorption of Au and TiO_2 NPs onto silica spheres with exposure to CPL. In this case, there was no difference in the photocatalytic response when the catalyst was irradiated with LCP or RCP light (Figure S9). All these data clearly demonstrate that the chiroptical activity associated with substrate-directed asymmetric plasmonic coupling can affect the population of generated hot carriers. Consequently, only a match between the helicity of the incoming CPL and the handedness of the substrate can induce the efficient activation of charges that translates to phototransformation of the polycyclic aromatic molecule through the activity of ROS.

To reiterate, we think that the different magnitude (~1000-fold) between the optical g-factors and the photochemical responses in our experiments may be the result of photochemical amplification through the steady-state generation of ROS, leading to the enrichment of an intrinsically small stereochemical bias (in this

case, the relatively small chiroptical activities of our photocatalysts). In parallel to this, enantioselective amplification and autocatalytic effects are well documented in the literature, being particularly relevant in biological homochirality.[37–39] Therefore, the role played by the autocatalytic generation of ROS as one more factor behind the photochemical bias cannot be discarded under the experimental conditions presented herein and should be investigated further.[40–42] Importantly, the polarization-dependent photochemical output is observed consistently by us in a complete set of experiments, for the L-SiO_2@Au@TiO_2 and R-SiO_2@Au@TiO_2 nanoribbons and the experiment with alternating polarizers (Figure 2e).

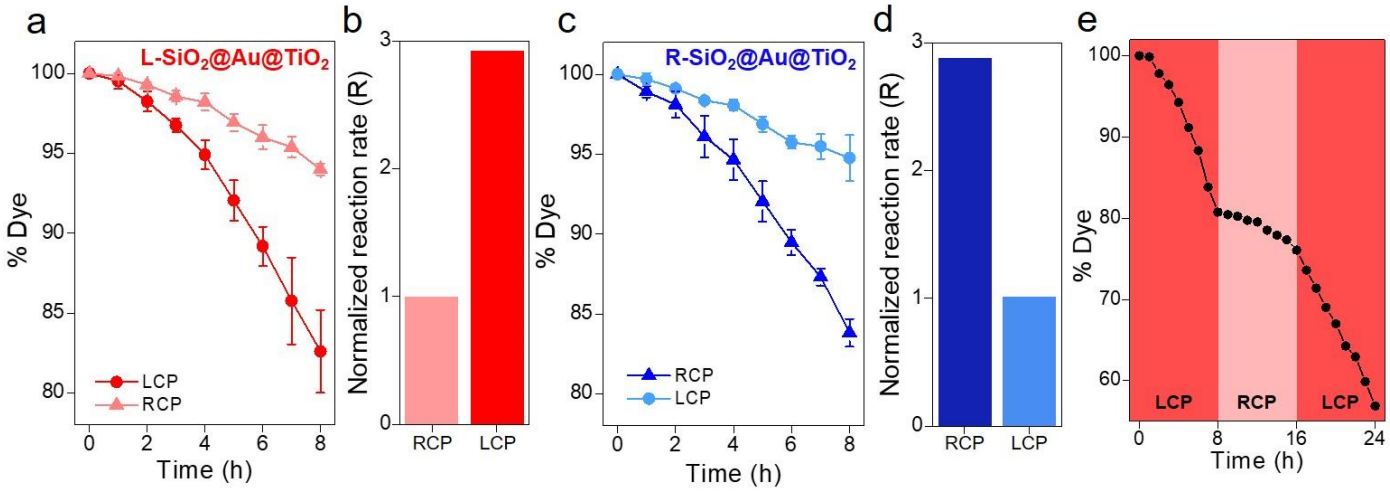

Figure 2. Photocatalytic activity of the hybrid nanoribbons as a function of CPL. (a, c) Photodegradation profiles of RhB in the presence of a chiral catalyst with either LCP or RCP light. The light source is a 150 W SLS401 xenon short-arc modified with CPL filters in the 400–800 nm range and the reaction time is 8 hours. The experiments are performed at a controlled temperature of 20 ºC. The experiment has been repeated 3 times for L-SiO_2@Au@TiO_2 and 2 times for R-SiO_2@Au@TiO_2. (b, d) Normalized reaction rates derived from the photodegradation profiles assuming a linear fit with $Rate_{experimental}$ = ΔAbsorbance/Δt, where Δt = 8 hours. (e) Photodegradation profile of RhB in the presence of the L-SiO_2@Au@TiO_2 nanoribbon using different polarizers (left circular polarizer in red and right circular polarizer in pink).

The development of a theoretical model allowed us to correlate the polarization-dependent photocatalytic properties of the inorganic hybrid nanoribbons with the generation of hot carriers at the metal-semiconductor interface. Upon electromagnetic activation, the Fermi sea of electrons of a metal NP is excited, leading to an out-of-equilibrium population of electrons. This distribution is divided in two different populations: (1) the low-energy electrons with energies close to the Fermi level of the metal (Drude electrons, Figure 3a, b) and

(2) the high energy electrons with $E_F < E < E_F + \hbar\omega$ (hot electrons, Figure 3a, b).[6] The latter population can be transferred across a Schottky barrier provided that the correct energy balance exists between the Fermi level of the metal and the conduction band of the semiconductor (Figure 3a). Accordingly, using the geometrical model described before as a starting point and then incorporating the quantum formalism that we developed in previous works,[15,43,44] we studied the surface-assisted generation of hot electrons created at the Au-TiO_2 interface. For more details on the model used, please refer to the SI. The spectrum calculated for the hot-electron generation rate excited with unpolarized light exhibits a strong plasmon peak at 580 nm originating from the plasmonic field enhancement effect (Figure 3c).[45] Such distribution reproduces qualitatively the absorption signature obtained experimentally (Figure 1d), with an asymmetric response that arises due to the uneven gaps between resonators in the 3D assembly. In our hot-electron generation mechanism, the electric fields inside the NPs generate energetic over-barrier electrons near the NP interface that are subsequently injected into the TiO_2 component (Figures 3a, b). Furthermore, the g-factors of the hot-electron generation (the ratio between the hot electron CD and the total hot electron rate) for both enantiomers present a profile that reproduces exactly the chiroptical activity of the hybrids (Figure 3d). Indeed, the population of excited electrons generated upon activation with CPL exhibits a chiral asymmetric behavior that is sensitive to the polarization of the light, and this chiral property could enable polarization-sensitive photocatalysis. Two absolute-value maxima can be observed for each type of nanoribbon at 560 and 595 nm. These theoretical predictions are in qualitative agreement with the experimental data (Figure 1e), showing once again that the density of the photogenerated hot carriers is directly related to whether the polarization of the light and the handedness of the helical NP assembly match. Moreover, it is interesting to look at the local properties of hot-electron generation since previous works have demonstrated that the electromagnetic field enhancement created at interparticle gaps can enhance significantly the generation of hot electrons at the metal-semiconductor interface.[10] Figures 3e and S10 show the calculated local properties of the R-ribbon model (this helicity is representative for both enantiomers) under directional CPL excitation in the vicinity of the plasmon resonance, with the K-vector parallel to the main axis of the helix (K||+z). Figure 3e demonstrates the generation of strong electromagnetic fields at the gaps between Au NPs only in that geometry in which the polarization of the directional excitation matches the handedness of the substrate. Moreover, Figure S10a shows both the local hot-electron generation rates and their local CDs for the right-handed Au NP assembly.

The presence of hot spots in these modeled assemblies indicate that the local hot-electron generation rates are different for the LCP and RCP excitations (Figure S10b). The simulated local hot electron CD signals also reveal the presence of localized hot spots in which the local CD is strongly enhanced; such regions make crucial contributions to the integrated hot electron CD signal, since the electromagnetic field enhancement normal to the metal-semiconductor interface is directly proportional to the rate of hot-electron generation (Figure S10c). To verify that the optoelectronic CD signals related to hot electrons originate from the chiral geometry, we performed a calculation on an achiral object as a control. For simplicity, spherical Au NPs with a diameter of 11 nm were chosen as the model system (Figures S10a and S11). As expected, both the integrated rates and the local responses show no CD since the object is both nonchiral and isotropic. Based on our theoretical model, we can conclude that the complex interparticle coupling produced in the chiral geometry results in an increase of the local electromagnetic field that depends on the helicity of CPL. As a consequence, the hot-electron generation derived from such interaction is polarization-dependent.

It is interesting to compare our finding with the chiral solid-state experiments on hot electron photocurrents in planar metastructures under normal incidence since the present study is focused on a different paradigm.[17,18] In contrast to the unidirectional excitation (normal incidence) and oriented nanocrystals in a typical photodetector experiment, here we discuss the ability of hot charge carriers excited on chiroptical plasmonic systems to generate polarization-dependent photocatalytic applications in solution, where the nanostructures present random orientations. This is a fundamentally different setting as far as the optical activity is concerned.[15,16,46] As explained above, this idea could have important implications in photocatalysis, as it allows us to utilize CPL as a tool to control chemical reactivity. Moreover, we believe that this work can be the first step towards more efficient chiral plasmonic photocatalysis at the molecular level.[37]

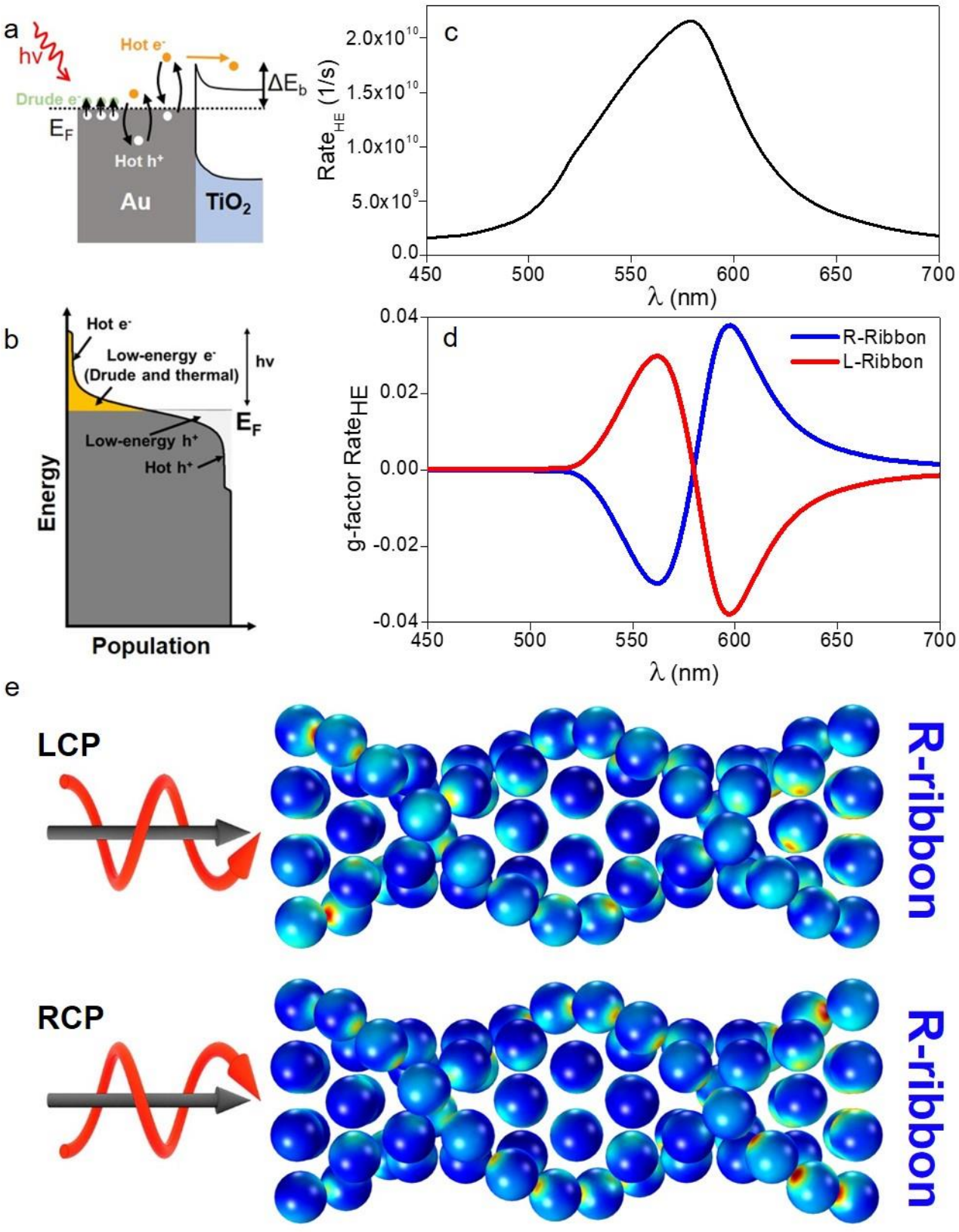

Figure 3. Theoretical description of the polarization-dependent hot-electron generation rate. (a) Schematic representation of the mechanism of hot electron injection at the Au-TiO_2 Schottky barrier. (b) Representation of the distribution of excited charges in the optically driven Fermi sea of electrons inside a plasmonic NP. (c) Rate of hot-electron generation for a Au NP helical assembly when excited with unpolarized light. (d)

Calculated rates of hot-electron generation for the Au NP helical assemblies when excited with CPL. The blue and red spectra correspond to the R- and L-enantiomers, respectively. The g-factor corresponds to the ratio between the hot electron CD and the total hot-electron generation rate. (e) Near-field enhancement map for the R-ribbon excited with LCP and RCP light. The formation of hot spots between neighboring NPs can be observed only when the polarization of light matches the helicity of the silica nanoribbon. The refractive index in these calculations is n=1.45.

Conclusions: Little experimental evidence existed with respect to the ability of plasmonic hot carriers to induce polarization-dependent photocatalytic reactions. In this work, we studied the photocatalytic activity of Au-TiO_2 nanohybrids assembled onto chiral silica nanoribbons. The unique geometry of these materials, together with the optical coupling between Au NPs, leads to chiroptical activity in the visible region of the electromagnetic spectrum. Consequently, when the hybrids are excited with CPL, the formation of hot carriers is polarization-dependent in nature with respect to the helicity of the electromagnetic field. Namely, substantial photocatalytic activity of SiO_2@Au@TiO_2 nanoribbons is observed only when excited with CPL that matches its handedness, in contrast to the residual activity observed when the same material is excited with CPL of the opposite polarization. Both experimental data and theoretical models demonstrate that this asymmetric photocatalytic feature is the result of the polarization-sensitive nature of the hot carriers generated during the electromagnetic excitation of the SiO_2@Au@TiO_2 hybrid. Taking into account that our experimental and theoretical methods can be extrapolated to other systems and photochemical reactions, we believe that these results can facilitate the investigation of new asymmetric photocatalytic phenomena induced by plasmonic excitation, together with the development of new colloidal strategies for the photoinduced growth of chiral structures.

Additional information

The Supporting Information is available free of charge on the ACS Publications website at DOI: XXXX

Experimental and theoretical methods; optical and photochemical g-factors; TEM characterization; photochemical tests and control experiments; theoretical hot electron generation rates.

Author information

Corresponding authors

*E-mail: miguel.comesana-hermo@u-paris.fr

*E-mail: govorov@ohiou.edu

*E-mail: macorrea@uvigo.es

ORCID

Yoel Negrín-Montecelo: 0000-0002-0977-7014
Artur Movsesyan: 0000-0002-5425-7747
Jie Gao: 0000-0002-8845-5450
Sven Burger: 0000-0002-3140-5380
Zhiming Wang: 0000-0003-2945-4834
Sylvain Nlate: 0000-0002-0300-9081
Emilie Pouget: 0000-0002-3175-6201
Reiko Oda: 0000-0003-3273-8635
Miguel Comesaña-Hermo: 0000-0001-8471-5510
Alexander O. Govorov: 0000-0003-1316-6758
Miguel A. Correa-Duarte: 0000-0003-1950-1414

Competing interests

The authors declare no competing financial interests.

Acknowledgments

M.C.-H. is funded by the CNRS Energy Unit (Cellule Energie) through the project PEPS-CHEAP. A.O.G. acknowledges generous support from the United States-Israel Binational Science Foundation (BSF) and the Nanoscale and Quantum Phenomena Institute at Ohio University. A.M. and Z.W. acknowledge the National Key Research and Development Program of China (2019YFB2203400) and the "111 Project" (B20030). S.B. acknowledges funding by the Deutsche Forschungsgemeinschaft (DFG, German Research Foundation) under Germany´s Excellence Strategy – The Berlin Mathematics Research Center MATH+ (EXC-2046/1, project ID: 390685689). J.G. is supported by the Chinese Scholarship Council Fellowship and the LabEx AMADEus (ANR-10-LABX-42) in the framework of IdEx Bordeaux (ANR-10-IDEX-03-02), i.e., the Investissements d'Avenir program of the French government managed by the Agence Nationale de la Recherche. M.A.C.-D. acknowledges financial support from the Spanish Ministerio de Economía y Competitividad under grant PID2020-113704RB-I00, Xunta de Galicia/FEDER (IN607A 2018/5 and Centro Singular de Investigación de

Galicia, Acc. 2019-2022, ED431G 2019-06), 0712_ACUINANO_1_E, 0624_2IQBIONEURO_6_E cofounded by FEDER through the program Interreg V-A España-Portugal (POCTEP) and NANOCULTURE (ERDF: 1.102.531) Interreg Atlantic Area, the European Union (European Regional Development Fund-ERDF).The authors thank Eugenio Solla and Miguel Spuch-Calvar (Universidade de Vigo) for assistance with electron microscopy measurements and for the design of original illustrations, respectively.

References

(1) Zhang, Y.; He, S.; Guo, W.; Hu, Y.; Huang, J.; Mulcahy, J. R.; Wei, W. D. Surface-Plasmon-Driven Hot Electron Photochemistry. *Chem. Rev.* **2018**, *118*, 2927–2954.

(2) Aslam, U.; Rao, V. G.; Chavez, S.; Linic, S. Catalytic Conversion of Solar to Chemical Energy on Plasmonic Metal Nanostructures. *Nat. Catal.* **2018**, *1*, 656–665.

(3) Zhou, L.; Swearer, D. F.; Zhang, C.; Robatjazi, H.; Zhao, H.; Henderson, L.; Dong, L.; Christopher, P.; Carter, E. A.; Nordlander, P.; Halas, N. J. Quantifying Hot Carrier and Thermal Contributions in Plasmonic Photocatalysis. *Science* **2018**, *362*, 69–72.

(4) Yu, S.; Wilson, A. J.; Heo, J.; Jain, P. K. Plasmonic Control of Multi-Electron Transfer and C-C Coupling in Visible-Light-Driven CO_2 Reduction on Au Nanoparticles. *Nano Lett.* **2018**, *18*, 2189–2194.

(5) Liu, J.; Feng, J.; Gui, J.; Chen, T.; Xu, M.; Wang, H.; Dong, H.; Chen, H.; Li, X.; Wang, L.; et al. Metal@semiconductor Core-Shell Nanocrystals with Atomically Organized Interfaces for Efficient Hot Electron-Mediated Photocatalysis. *Nano Energy* **2018**, *48*, 44–52.

(6) Sousa-Castillo, A.; Comesaña-Hermo, M.; Rodríguez-González, B.; Pérez-Lorenzo, M.; Wang, Z.; Kong, X.-T.; Govorov, A. O.; Correa-Duarte, M. A. Boosting Hot Electron-Driven Photocatalysis through Anisotropic Plasmonic Nanoparticles with Hot Spots in Au-TiO_2 Nanoarchitectures. *J. Phys. Chem. C* **2016**, *120*, 11690–11699.

(7) Tatsuma, T.; Nishi, H.; Ishida, T. Plasmon-Induced Charge Separation: Chemistry and Wide Applications. *Chem. Sci.* **2017**, *8*, 3325–3337.

(8) Clavero, C. Plasmon-Induced Hot-Electron Generation at Nanoparticle/Metal-Oxide Interfaces for Photovoltaic and Photocatalytic Devices. *Nat. Photonics* **2014**, *8*, 95–103.

(9) Pensa, E.; Gargiulo, J.; Lauri, A.; Schlücker, S.; Cortés, E.; Maier, S. A. Spectral Screening of the Energy of Hot Holes over a Particle Plasmon Resonance. *Nano Lett.* **2019**, *19*, 1867–1874.

(10) Negrín-Montecelo, Y.; Comesaña-Hermo, M.; Kong, T.; Rodríguez-González, B.; Wang, Z.; Pérez-Lorenzo, M.; Govorov, A. O.; Correa-Duarte, M. A. Traveling Hot-Spots in Plasmonic Photocatalysts: Manipulating Interparticle Spacing for Real-Time Control of Electron Injection. *ChemCatChem* **2018**, *10*, 1561–1565.

(11) Lee, H. E.; Ahn, H. Y.; Mun, J.; Lee, Y. Y.; Kim, M.; Cho, N. H.; Chang, K.; Kim, W. S.; Rho, J.; Nam, K. T. Amino-Acid- and Peptide-Directed Synthesis of Chiral Plasmonic Gold Nanoparticles. *Nature* **2018**, *556*, 360–364.

(12) González-Rubio, G.; Mosquera, J.; Kumar, V.; Pedrazo-Tardajos, A.; Llombart, P.; Solís, D. M.; Lobato, I.; Noya, E. G.; Guerrero-Martínez, A.; Taboada, J. M.; Obelleiro, F.; MacDowell, L. G.; Bals, S.; Liz-Marzán, L. M. Micelle-Directed Chiral Seeded Growth on Anisotropic Gold Nanocrystals. *Science (80-.).* **2020**, *368*, 1472–1477.

(13) Cheng, J.; Le Saux, G.; Gao, J.; Buffeteau, T.; Battie, Y.; Barois, P.; Ponsinet, V.; Delville, M. H.; Ersen, O.; Pouget, E.; Oda, R. GoldHelix: Gold Nanoparticles Forming 3D Helical Superstructures with Controlled Morphology and Strong Chiroptical Property. *ACS Nano* **2017**, *11*, 3806–3818.

(14) Kuzyk, A.; Schreiber, R.; Fan, Z.; Pardatscher, G.; Roller, E. M.; Högele, A.; Simmel, F. C.; Govorov, A. O.; Liedl, T. DNA-Based Self-Assembly of Chiral Plasmonic Nanostructures with Tailored Optical Response. *Nature* **2012**, *483*, 311–314.

(15) Liu, T.; Besteiro, L. V.; Liedl, T.; Correa-Duarte, M. A.; Wang, Z.; Govorov, A. O. Chiral Plasmonic Nanocrystals for Generation of Hot Electrons: Toward Polarization-Sensitive Photochemistry. *Nano Lett.* **2019**, *19*, 1395–1407.

(16) Khorashad, L. K.; Besteiro, L. V.; Correa-Duarte, M. A.; Burger, S.; Wang, Z. M.; Govorov, A. O. Hot Electrons Generated in Chiral Plasmonic Nanocrystals as a Mechanism for Surface

Photochemistry and Chiral Growth. *J. Am. Chem. Soc.* **2020**, *142*, 4193–4205.

(17) Fang, Y.; Verre, R.; Shao, L.; Nordlander, P.; Käll, M. Hot Electron Generation and Cathodoluminescence Nanoscopy of Chiral Split Ring Resonators. *Nano Lett.* **2016**, *16*, 5183–5190.

(18) Li, W.; Coppens, Z. J.; Besteiro, L. V.; Wang, W.; Govorov, A. O.; Valentine, J. Circularly Polarized Light Detection with Hot Electrons in Chiral Plasmonic Metamaterials. *Nat. Commun.* **2015**, *6*, 8379.

(19) Zheng, G.; He, J.; Kumar, V.; Wang, S.; Pastoriza-Santos, I.; Pérez-Juste, J.; Liz-Marzán, L. M.; Wong, K.-Y. Discrete Metal Nanoparticles with Plasmonic Chirality. *Chem. Soc. Rev.* **2021**, *50*, 3738–3754.

(20) Ma, W.; Xu, L.; De Moura, A. F.; Wu, X.; Kuang, H.; Xu, C.; Kotov, N. A. Chiral Inorganic Nanostructures. *Chem. Rev.* **2017**, *117*, 8041–8093.

(21) Hao, C.; Xu, L.; Ma, W.; Wu, X.; Wang, L.; Kuang, H.; Xu, C. Unusual Circularly Polarized Photocatalytic Activity in Nanogapped Gold-Silver Chiroplasmonic Nanostructures. *Adv. Funct. Mater.* **2015**, *25*, 5816–5822.

(22) Guerrero-Martínez, A.; Auguié, B.; Alonso-Gómez, J. L.; Džolič, Z.; Gómez-Graña, S.; Žinić, M.; Cid, M. M.; Liz-Marzán, L. M. Intense Optical Activity from Three-Dimensional Chiral Ordering of Plasmonic Nanoantennas. *Angew. Chemie - Int. Ed.* **2011**, *50*, 5499–5503.

(23) Ben-Moshe, A.; Maoz, B. M.; Govorov, A. O.; Markovich, G. Chirality and Chiroptical Effects in Inorganic Nanocrystal Systems with Plasmon and Exciton Resonances. *Chem. Soc. Rev.* **2013**, *42*, 7028–7041.

(24) Lu, J.; Xue, Y.; Bernardino, K.; Zhang, N. N.; Gomes, W. R.; Ramesar, N. S.; Liu, S.; Hu, Z.; Sun, T.; de Moura, A. F.; Kotov, N. A.; Liu, K. Enhanced Optical Asymmetry in Supramolecular Chiroplasmonic Assemblies with Long-Range Order. *Science* **2021**, *371*, 1368–1374.

(25) Lewandowski, W.; Szustakiewicz, P.; Kowalska, N.; Grzelak, D.; Narushima, T.; Góra, M.; Bagiński, M.; Pociecha, D.; Okamoto, H.; Liz-Marzán, L. M. Supramolecular Chirality Synchronization in Thin Films of Plasmonic Nanocomposites. *ACS Nano* **2020**, *14*, 12918–12928.

(26) Saito, K.; Tatsuma, T. Chiral Plasmonic Nanostructures Fabricated by Circularly Polarized Light. *Nano Lett.* **2018**, *18*, 3209–3212.

(27) Okazaki, Y.; Cheng, J.; Dedovets, D.; Kemper, G.; Delville, M. H.; Durrieu, M. C.; Ihara, H.; Takafuji, M.; Pouget, E.; Oda, R. Chiral Colloids: Homogeneous Suspension of Individualized SiO_2 Helical and Twisted Nanoribbons. *ACS Nano* **2014**, *8*, 6863–6872.

(28) Delclos, T.; Aimé, C.; Pouget, E.; Brizard, A.; Huc, I.; Delville, M. H.; Oda, R. Individualized Silica Nanohelices and Nanotubes: Tuning Inorganic Nanostructures Using Lipidic Self-Assemblies. *Nano Lett.* **2008**, *8*, 1929–1935.

(29) Nguyen, L.; Dass, M.; Ober, M. F.; Besteiro, L. V.; Wang, Z. M.; Nickel, B.; Govorov, A. O.; Liedl, T.; Heuer-Jungemann, A. Chiral Assembly of Gold-Silver Core-Shell Plasmonic Nanorods on DNA Origami with Strong Optical Activity. *ACS Nano* **2020**, *14*, 7454–7461.

(30) Kong, X. T.; Besteiro, L. V.; Wang, Z.; Govorov, A. O. Plasmonic Chirality and Circular Dichroism in Bioassembled and Nonbiological Systems: Theoretical Background and Recent Progress. *Adv. Mater*. **2020**, *32*, 1801790.

(31) Lee, S. A.; Link, S. Chemical Interface Damping of Surface Plasmon Resonances. *Acc. Chem. Res*. **2021**, *54*, 1950–1960.

(32) Pomplun, J.; Burger, S.; Zschiedrich, L.; Schmidt, F. Adaptive Finite Element Method for Simulation of Optical Nano Structures. *Phys. Status Solidi B* **2007**, *244*, 3419–3434.

(33) Sousa-Castillo, A.; Couceiro, J. R.; Tomás-Gamasa, M.; Mariño-López, A.; López, F.; Baaziz, W.; Ersen, O.; Comesaña-Hermo, M.; Mascareñas, J. L.; Correa-Duarte, M. A. Remote Activation of Hollow Nanoreactors for Heterogeneous Photocatalysis in Biorelevant Media. *Nano Lett.* **2020**, *20*, 7068–7076.

(34) Inoue, Y.; Tsuneishi, H.; Hakushi, T.; Yagi, K.; Awazu, K.; Onuki, H. First Absolute Asymmetric Synthesis with Circularly Polarized Synchrotron Radiation in the Vacuum Ultraviolet Region: Direct Photoderacemization of (E)-Cyclooctene. *Chem. Commun.* **1996**, *1*, 2627–2628.

(35) Feringa, B.; Delden, R. Absolute Asymmetric Synthesis: The Origin, Control and Amplification of Chirality. *Angew. Chem. Int. Ed.* **1999**, *38*, 3418–3438.

(36) Baffou, G.; Bordacchini, I.; Baldi, A.; Quidant, R. Simple Experimental Procedures to Distinguish Photothermal from Hot-Carrier Processes in Plasmonics. *Light Sci. Appl.* **2020**, *9*, 108.

(37) Inoue, Y.; Ramamurthy, V. *Chiral Photochemistry*; CRC Press: Boca Raton, 2004.

(38) Soai, K.; Sato, I.; Shibata, T. Asymmetric Autocatalysis and the Origin of Chiral Homogeneity in Organic Compounds. *Chem. Rec.* **2001**, *1*, 321–332.

(39) Soai, K.; Kawasaki, T.; Matsumoto, A. Asymmetric Autocatalysis of Pyrimidyl Alkanol and Its Application to the Study on the Origin of Homochirality. *Acc. Chem. Res.* **2014**, *47*, 3643–3654.

(40) Durantini, A. M.; Greene, L. E.; Lincoln, R.; Martínez, S. R.; Cosa, G. Reactive Oxygen Species Mediated Activation of a Dormant Singlet Oxygen Photosensitizer: From Autocatalytic Singlet Oxygen Amplification to Chemicontrolled Photodynamic Therapy. *J. Am. Chem. Soc.* **2016**, *138*, 1215–1225.

(41) Hui, P.; Branca, M.; Limoges, B.; Mavré, F. An Autocatalytic Organic Reaction Network Based on Cross-Catalysis. *Chem. Commun.* **2021**, *57*, 11374–11377.

(42) Corvalán, N. A.; Caviglia, A. F.; Felsztyna, I.; Itri, R.; Lascano, R. Lipid Hydroperoxidation Effect on the Dynamical Evolution of the Conductance Process in Bilayer Lipid Membranes: A Condition Toward Criticality. *Langmuir* **2020**, *36*, 8883–8893.

(43) Hartland, G. V.; Besteiro, L. V.; Johns, P.; Govorov, A. O. What's so Hot about Electrons in Metal Nanoparticles? *ACS Energy Lett.* **2017**, *2*, 1641–1653.

(44) Santiago, E. Y.; Besteiro, L. V.; Kong, X.-T.; Correa-Duarte, M. A.; Wang, Z.; Govorov, A. O. Efficiency of Hot-Electron Generation in Plasmonic Nanocrystals with Complex Shapes: Surface-Induced Scattering, Hot Spots, and Interband Transitions. *ACS Photonics* **2020**, *7*, 2807–2824.

(45) Besteiro, L. V.; Kong, X.-T.; Wang, Z.; Hartland, G.; Govorov, A. O. Understanding Hot-Electron Generation and Plasmon Relaxation in Metal Nanocrystals: Quantum and Classical Mechanisms. *ACS*

Photonics **2017**, *4*, 2759–2781.

(46) Fasman, G. D. *Circular Dichroism and the Conformational Analysis of Biomolecules*; Springer US: New York, 1996.

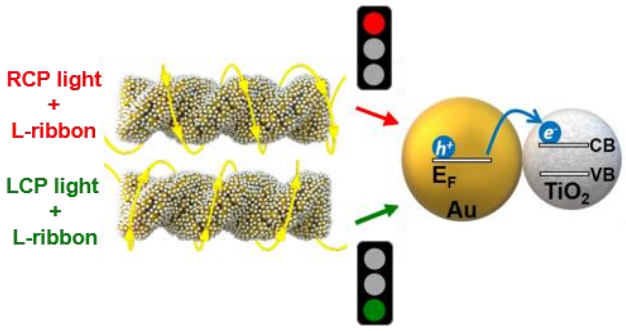

TOC Graphic